- The NiCEST Approach: Nickel(II) ParaCEST MRI Contrast Agents
  Olatunde, A. O.; Dorazio, S. J.; Spernyak, J. A.; Morrow, J. R. *J. Am. Chem. Soc.* **2012**, *134*, 18503–18505.
  Abstract:

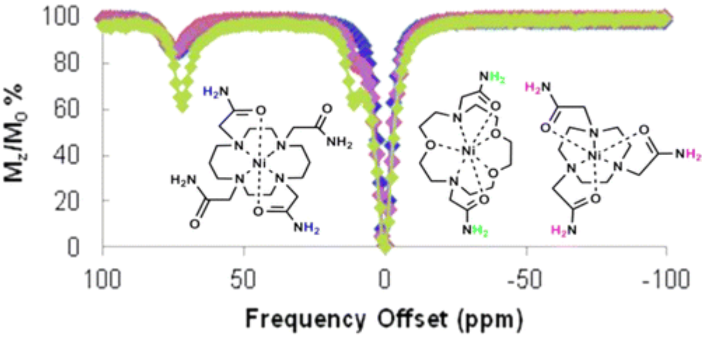

Paramagnetic Ni(II) complexes are shown here to form paraCEST MRI contrast agents (paraCEST = paramagnetic chemical exchange saturation transfer; NiCEST = Ni(II) based CEST agents). Three azamacrocycles with amide pendent groups bind Ni(II) to form stable NiCEST contrast agents including 1,4,7-tris(carbamoylmethyl)-1,4,7-triazacyclononane (**L1**), 1,4,8,11-tetrakis(carbamoylmethyl)-1,4,8,11-tetraazacyclotetradecane (**L2**), and 7,13-bis(carbamoylmethyl)-1,4,10-trioxa-7,13-diazacyclopentadecane (**L3**). [Ni(**L3**)]$^{2+}$, [Ni(**L1**)]$^{2+}$, and [Ni(**L2**)]$^{2+}$ have CEST peaks attributed to amide protons that are shifted 72, 76, and 76 ppm from the bulk water resonance, respectively. Both CEST MR images and CEST spectroscopy show that [Ni(**L3**)]$^{2+}$ has the largest CEST effect in 100 mM NaCl, 20 mM HEPES pH 7.4 at 37 °C. This larger CEST effect is attributed to the sharper proton resonances of the complex which arise from a rigid structure and low relaxivity.

- The Correct Structure of Aquatolide—Experimental Validation of a Theoretically-Predicted Structural Revision
  Lodewyk, M. W.; Soldi, C.; Jones, P. B.; Olmstead, M. M.; Rita, J.; Shaw, J. T.; Tantillo, D. J. *J. Am. Chem. Soc.* **2012**, *134*, 18550–18553.
  Abstract:

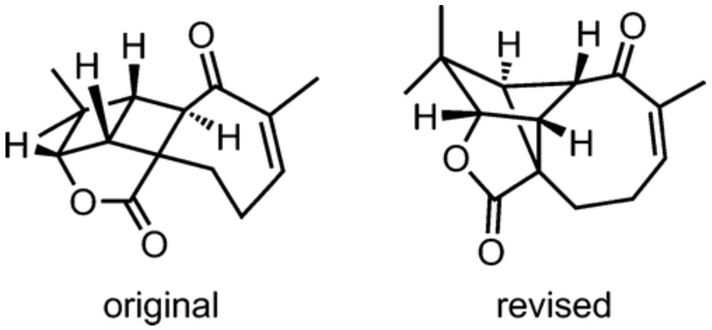

Aquatolide has been reisolated from its natural source, and its structure has been revised on the basis of quantum-chemical NMR calculations, extensive experimental NMR analysis, and crystallography.

- Designing Two Self-Assembly Mechanisms into One Viral Capsid Protein
  Van Eldijk, M. B.; Wang, J. C.-Y.; Minten, I. J.; Li, C.; Zlotnick, A.; Nolte, R. J. M.; Cornelissen, J. J. L. M.; Van Hest, J. C. M. *J. Am. Chem. Soc.* **2012**, *134*, 18506–18509.
  Abstract:

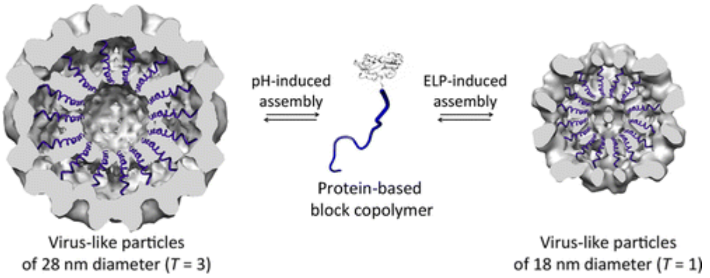

ELP-CP, a structural fusion protein of the thermally responsive elastin-like polypeptide (ELP) and a viral capsid protein (CP), was designed, and its assembly properties were investigated. Interestingly, this protein-based block copolymer could be self-assembled via two mechanisms into two different, well-defined nanocapsules: (1) pH-induced assembly yielded 28 nm virus-like particles, and (2) ELP-induced assembly yielded 18 nm virus-like particles. The latter were a result of the emergent properties of the fusion protein. This work shows the feasibility of creating a self-assembly system with new properties by combining two structural protein elements.

- Controlling the Degree of Polymerization, Bond Lengths, and Bond Angles of Plasmonic Polymers
  Lukach, A.; Liu, K.; Therien-Aubin, H.; Kumacheva, E. *J. Am. Chem. Soc.* **2012**, *134*, 18853–18859.
  Abstract:

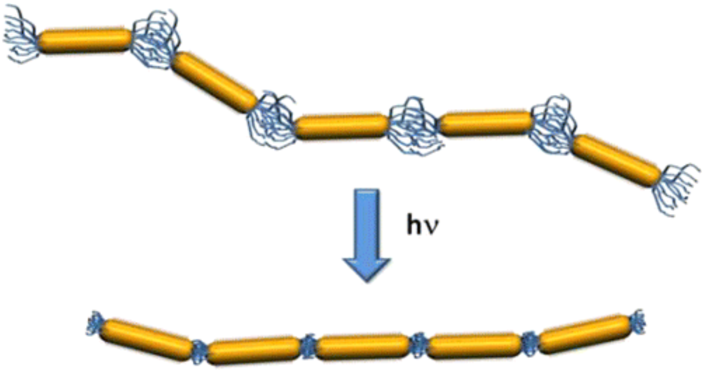

Plasmonic polymers present an interesting concept that builds on the analogy between molecular polymers and linear chains of strongly interacting metal nanoparticles. Ensemble-averaged optical properties of plasmonic polymers are strongly influenced by their structure. In the present work, we formed plasmonic polymers by using solution-based assembly of gold nanorods (NRs) end-tethered with photoactive macromolecular tethers. By using postassembly ligand photo-cross-linking, we established a method to arrest NR polymer growth after a particular self-assembly time, and in this manner, using kinetics of step-growth polymerization, we achieved control over the average degree of polymerization of plasmonic polymers. Photo-cross-linking of ligands also enabled control over the internanorod distance and resulted in the increased rigidity of NR chains. These results, along with a higher structural integrity of NR chains, can be utilized in plasmonic nanostructure engineering and facilitate advanced applications of plasmonic polymers in sensing and optoelectronics.

- Synthetic Lipid Membrane Channels Formed by Designed DNA Nanostructures
  Langecker, M.; Arnaut, V.; Martin, T. G.; List, J.; Renner, S.; Mayer, M.; Dietz, H.; Simmel, F. C. *Science* **2012**, *338*, 932-936.
  Abstract:

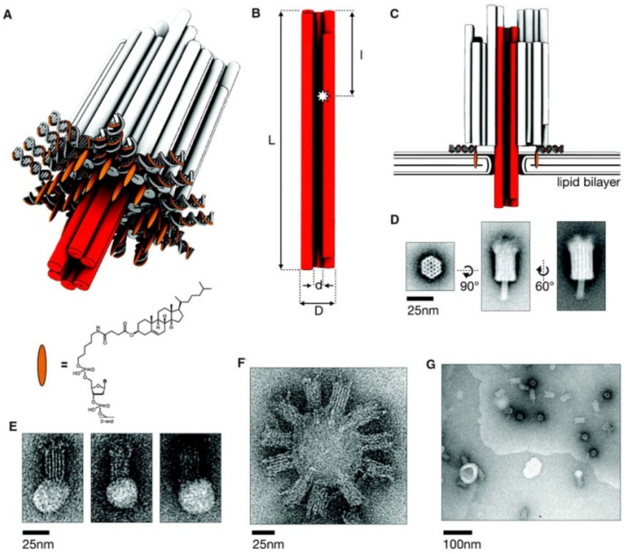

We created nanometer-scale transmembrane channels in lipid bilayers by means of self-assembled DNA-based nanostructures. Scaffolded DNA origami was used to create a stem that penetrated and spanned a lipid membrane, as well as a barrel-shaped cap that adhered to the membrane, in part via 26 cholesterol moieties. In single-channel electrophysiological measurements, we found similarities to the response of natural ion channels, such as conductances on the order of 1 nanosiemens and channel gating. More pronounced gating was seen for mutations in which a single DNA strand of the stem protruded into the channel. Single-molecule translocation experiments show that the synthetic channels can be used to discriminate single DNA molecules.

- Brønsted basicity of the air-water interface.
  Mishra, H.; Enami, S.; Nielsen, R. J.; Stewart, L. A.; Hoffmann, M. R.; Goddard III, W. A.; Colussia, A. J. *Proc. Nat. Acad. Sci. USA* **2012**, *109*, 18679-18683.
  Abstract:

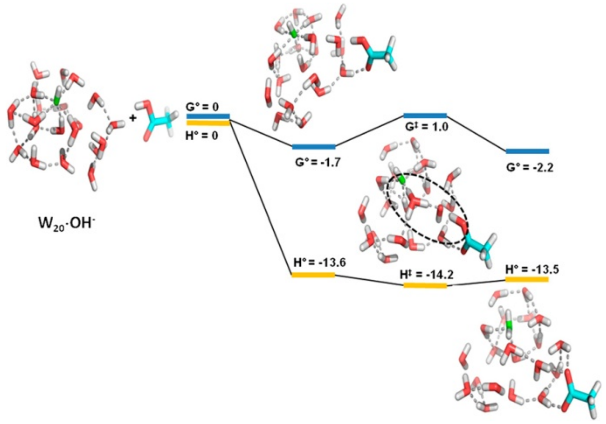

Differences in the extent of protonation of functional groups lying on either side of water-hydrophobe interfaces are deemed essential to enzymatic catalysis, molecular recognition, bioenergetic transduction, and atmospheric aerosol-gas exchanges. The sign and range of such differences, however, remain conjectural. Herein we report experiments showing that gaseous carboxylic acids RCOOH(g) begin to deprotonate on the surface of water significantly more acidic than that supporting the dissociation of dissolved acids RCOOH(aq). Thermodynamic analysis indicates that > 6 H_2O molecules must participate in the deprotonation of RCOOH(g) on water, but quantum mechanical calculations on a model air-water interface predict that such event is hindered by a significant kinetic barrier unless OH^- ions are present therein. Thus, by detecting $RCOO^-$ we demonstrate the presence of OH^- on the aerial side of on pH > 2 water exposed to RCOOH(g). Furthermore, because in similar experiments the base $(Me)_3N$(g) is protonated only on pH < 4 water, we infer that the outer surface of water is Brønsted neutral at pH ~3 (rather than at pH 7 as bulk water), a value that matches the isoelectric point of bubbles and oil droplets in independent electrophoretic experiments. The OH^- densities sensed by RCOOH(g) on the aerial surface of water, however, are considerably smaller than those at the (>1 nm) deeper shear planes probed in electrophoresis, thereby implying the existence of OH^- gradients in the interfacial region. This fact could account for the weak OH^- signals detected by surface-specific spectroscopies.

- Fluorescent differentiation and quantificational detection of free tryptophan in serum within a confined metal–organic tetrahedron
  He, C.; Wang, J.; Wu, P.; Jia, L.; Bai, Y.; Zhang, Z.; Duan, C. *Chem. Commun.* **2012,** *48,* 11880–11882.
  Abstract:

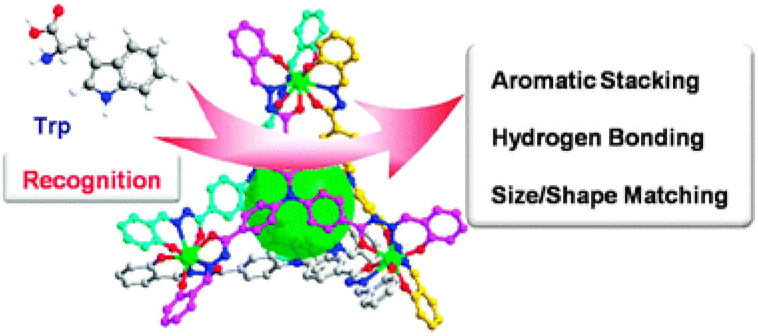

A metal–organic cerium tetrahedron having size constraints and cooperated interactions within its cavity was used to selectively recognize tryptophan over other natural amino acids and Trp-containing peptides. It was applied in quantificational detection of free tryptophan in serum.

- Reversible binding of nitric oxide to an Fe(III) complex of a tetra-amido macrocycle
  Pluth M. D.; Lippard, S. J. *Chem. Commun.* **2012,** *48,* 11981–11983.
  Abstract:

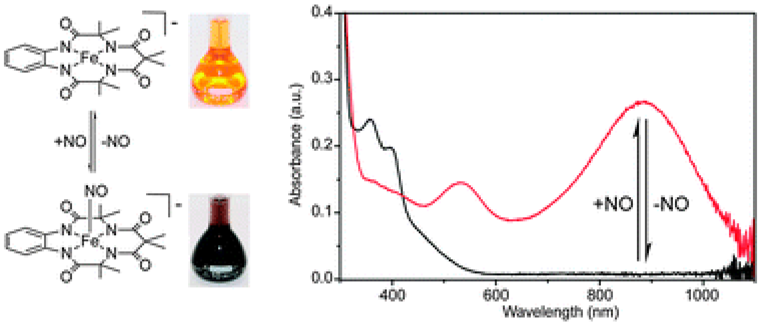

Nitric oxide binds reversibly to the Fe(III) complex of a well-developed tetra-amido macrocyclic ligand. Reaction with NO results in formation of a species consistent with an *S* = 1 $\{Fe–NO\}^6$ ground state as characterized by UV-vis, IR, EPR, and Mössbauer spectroscopy. The resultant nitrosyl is labile and dissociates readily upon purging with N_2, thus providing a rare example of reversible NO binding to non-heme iron.

- A Tri-copper(II) Complex Displaying DNA-Cleaving Properties and Antiproliferative Activity

against Cancer Cells
Suntharalingam, K.; Hunt, D.J.; Duarte, A. A.; White, A. J. P.; Mann, D. J.; Vilar, R. *Chem. Eur. J.* **2012**, *19*, 15133–15141.
Abstract:

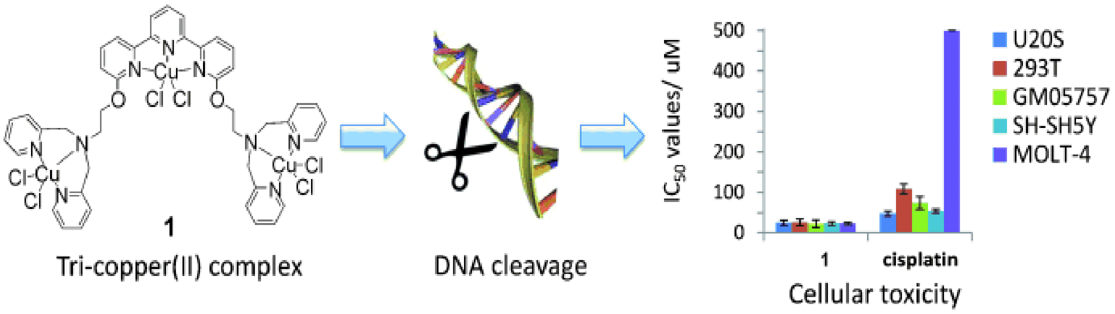

A new disubstituted terpyridine ligand and the corresponding tri-copper(II) complex have been prepared and characterised. The binding affinity and binding mode of this tri-copper complex (as well as the previously reported mono- and di-copper analogues) towards duplex DNA were determined by using UV/Vis spectroscopic titrations and fluorescent indicator displacement (FID) assays. These studies showed the three complexes to bind moderately (in the order of 10^4 M^{-1}) to duplex DNA (ct-DNA and a 26-mer sequence). Furthermore, the number of copper centres and the nature of the substituents were found to play a significant role in defining the binding mode (intercalative or groove binding). The nuclease potential of the three complexes was investigated by using circular plasmid DNA as a substrate and analysing the products by agarose-gel electrophoresis. The cleaving activity was found to be dependent on the number of copper centres present (cleaving potency was in the order: tri-copper>di-copper>mono-copper). Interestingly, the tri-copper complex was able to cleave DNA without the need of external co-reductants. As this complex displayed the most promising nuclease properties, cell-based studies were carried out to establish if there was a direct link between DNA cleavage and cellular toxicity. The tri-copper complex displayed high cytotoxicity against four cancer cell lines. Of particular interest was that it displayed high cytotoxicity against the cisplatin-resistant MOLT-4 leukaemia cell line. Cellular uptake studies showed that the tri-copper complex was able to enter the cell and more importantly localise in the nucleus. Immunoblotting analysis (used to monitor changes in protein levels related to the DNA damage response pathway) and DNA-flow cytometric studies suggested that this tri-copper(II) complex is able to induce cellular DNA damage.

- Formal Total Synthesis of Palmerolide A
  Pawar, A. B.; Prasad, K. R. *Chem. Eur. J.* **2012**, *19*, 15202–15206.
  Abstract:

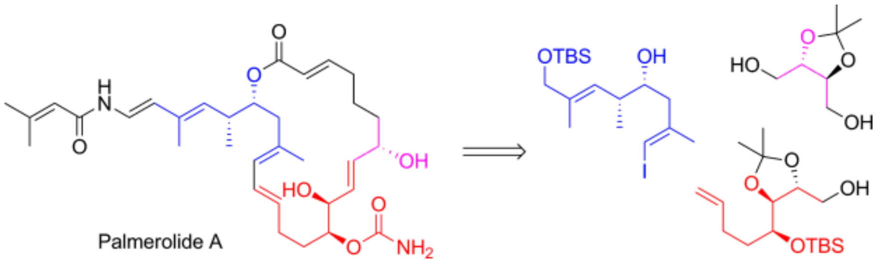

A formal total synthesis of the 20-membered marine macrolide, palmerolide A from chiral pool tartaric acid is described. Elaboration of a γ-hydroxy amide, which is derived from the desymmetrization of tartaric acid amide, and Boord olefination are the pivotal reactions employed

for the synthesis of the chiral building blocks, and Stille coupling and ring-closing metathesis (RCM) are used to assemble the macrolactone.

- Induction of the Columnar Phase of Unconventional Dendrimers by Breaking the C_2 Symmetry of Molecules
  Lai, L.-L.; Wang, S.-W.; Cheng, K.-L.; Lee, J.-J.; Wang, T.-H.; Hsu, H.-F. *Chem. Eur. J.* **2012**, 18, 15361–15367.
  Abstract:

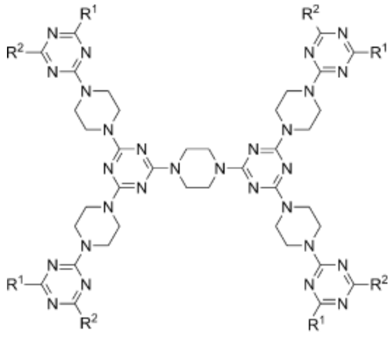

[2N(C$_8$)$_2$G$_2$N]$_2$; $R^1 = R^2 = N(C_8H_{15})_2$
[2N(C$_6$)$_2$G$_2$N]$_2$; $R^1 = R^2 = N(C_6H_{13})_2$
[N(C$_8$)$_2$OC$_8$G$_2$N]$_2$; $R^1 = N(C_8H_{15})_2$, $R^2 = OC_8H_{15}$
[N(C$_6$)$_2$OC$_6$G$_2$N]$_2$; $R^1 = N(C_6H_{13})_2$, $R^2 = OC_6H_{13}$

Broken symmetry: Unconventional triazine-based dendrimers (see figure) were prepared and, according to studies by differential scanning calorimetry, polarizing microscopy, and powder XRD, they display columnar liquid-crystalline (LC) phases. Simulations indicate that the conformations of the dendrimers are rather flat and disfavor formation of the LC phase. However, due to C_2-symmetry breaking, they have structural isomers in the solid state and thus show the desired columnar phases.

- Hydrophilicity Control of Visible-Light Hydrogen Evolution and Dynamics of the Charge-Separated State in Dye/TiO_2/Pt Hybrid Systems
  Han, W.-S.; Wee, K.-R.; Kim, H.-Y.; Pac, C.; Nabetani, Y.; Yamamoto, D.; Shimada, T.; Inoue, H.; Choi, H.; Cho, K.; Kang, S. O. *Chem. Eur. J.* **2012**, 18, 15368 – 15381.
  Abstract:

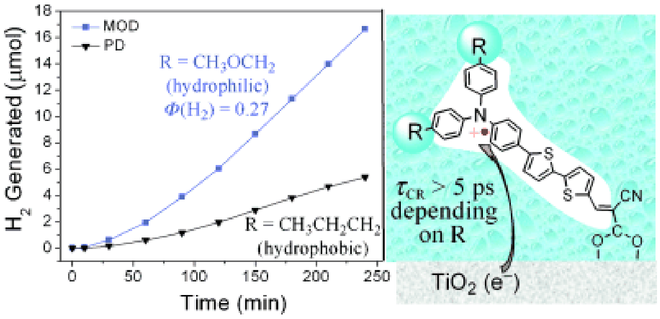

Photosensitized H_2 generation by a series of Dye/TiO_2/Pt hybrids revealed clear dependence on the hydrophilic/hydrophobic character of the substituent R of Dye (see figure; $\Phi(H_2)$=apparent quantum yield for H_2 generation.), which was shown by femtosecond transient spectroscopy to arise from the hydrophilic control of charge recombination (CR) between Dye.$^+$ and the injected electron $TiO_2(e^-)$.

- The Chameleonic Nature of Diazaperopyrenium Recognition Processes

Basuray, A. N.; Jacquot de Rouville, H.-P.; Hartlieb, K. J.; Kikuchi, T.; Strutt, N. L.; Bruns, C. J.; Ambrogio, M. W.; Avestro, A.-J.; Schneebeli, S. T.; Fahrenbach, A. C.; Stoddart, J. F. *Angew. Chem. Int. Ed.* **2012**, *51*, 11872–11877.

Abstract:

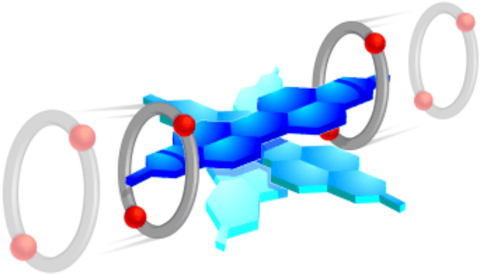

Two for the price of one! The diazaperopyrenium dication behaves dichotomously in a homo- and heterophilic manner, allowing for complexation with itself and a variety of π-electron-rich donors. This chameleonic characteristic, in addition to its electronic properties, leads to self-assembled nanowires in the solid state, as well as to its acting as a template for aromatic crown ethers to form a [3]- and two [2]rotaxanes (see picture).

- Tunable Supermicelle Architectures from the Hierarchical Self-Assembly of Amphiphilic Cylindrical B–A–B Triblock Co-Micelles
  Qiu, H.; Russo, G.; Rupar, P. A.; Chabanne, L.; Winnik, M. A.; Manners, I. (2012), *Angew. Chem. Int. Ed.* **2012**, *51*, 11882–11885.
  Abstract:

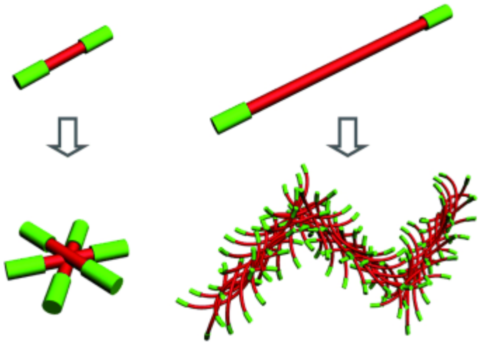

Crossing the block: Amphiphilic cylindrical B–A–B triblock co-micelles, micelle analogues of bolaamphiphiles, can be prepared by the crystallization-driven living self-assembly of diblock copolymers with core-forming polyferrocenylsilane blocks. These novel co-micelle building blocks form regular crossed or spherical supermicelles or elongated networks in polar media depending on the relative lengths of the A and B segments (see picture).

- Nanotechnology-Enabled Energy Harvesting for Self-Powered Micro-/Nanosystems
  Wang, Z. L.; Wu, W. *Angew. Chem. Int. Ed.* **2012**, *51*, 11700-11721.
  Abstract:

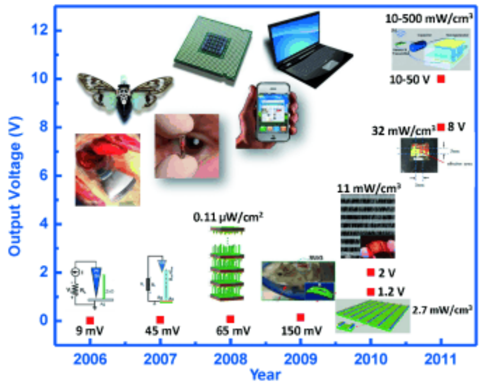

A bumper harvest, albeit on a small scale, is required for micro-/nanosystems (MNSs) to function reliably without an external power source. MNSs that can harvest energy from the environment in which they are used have wide-ranging potential applications in health, environmental, and infrastructure monitoring, as well as networking and defense technologies. This Review explores possibilities for energy harvesting to meet the future demand for MNSs.

- Pentaarylazafullerenes and their Triaryldihydro and Tetraarylmonohydro Precursors
  Neubauer, R., Heinemann, F. W., Hampel, F., Rubin, Y.; Hirsch, A. *Angew. Chem. Int. Ed.* **2012**, *51*, 11722–11726.
  Abstract:

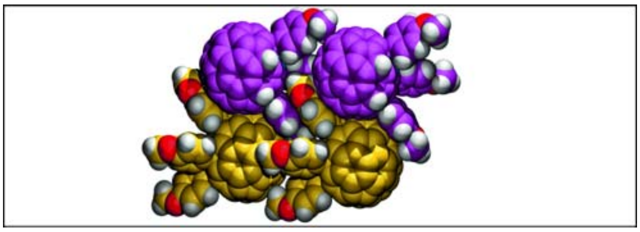

Give me five! The title compounds were isolated from the acid-catalyzed reaction of a C59N precursor with electron-rich aromatic compounds. Single-crystal X-ray diffraction on two compounds reveals characteristic packing motifs; the triaryldihydro derivative has a pseudo-stacked arrangement (C violet/yellow, N blue, O red, H white).

- Design Principles for Photovoltaic Devices Based on Si Nanowires with Axial or Radial p–n Junctions
  Christesen, J. D.; Zhang, X.; Pinion, C. W.; Celano, T. A.; Flynn, C. J.; Cahoon, J. F. *Nano Letters* **2012** *12*, 6024-6029.
  Abstract:

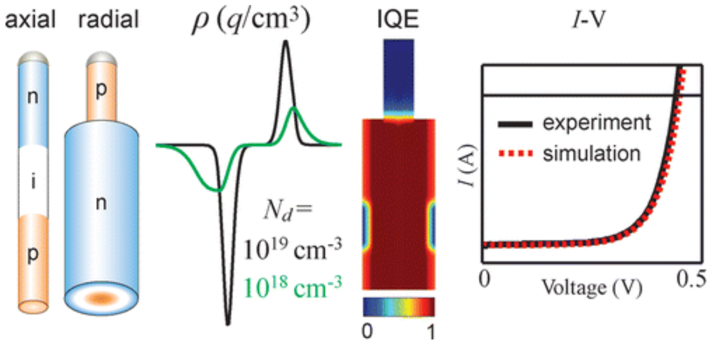

Semiconductor nanowires (NWs) are a developing platform for electronic and photonic technologies, and many demonstrated devices utilize a p-type/n-type (p–n) junction encoded along either the axial or radial directions of the wires. These miniaturized junctions enable a diverse range of functions, from sensors to solar cells, yet the physics of the devices has not been thoroughly evaluated. Here, we present finite-element modeling of axial and radial Si NW p–n junctions with total diameters of ∼240 nm and donor/acceptor doping levels ranging from 10^{16} to 10^{20} cm^{-3}. We evaluate the photovoltaic performance of horizontally oriented NWs under 1 sun illumination and compare simulated current–voltage data to experimental measurements, permitting detailed analysis of NW performance, limitations, and prospect as a technology for solar energy conversion. Although high surface-to-volume ratios are cited as detrimental to NW performance, radial p–n junctions are surprisingly insensitive to surface recombination, with devices supporting open-circuit voltages (V_{OC}) of ∼0.54 V and internal quantum efficiencies of 95% even with high surface recombination velocities (SRVs) of 10^5 cm/s. Axial devices, in which the depletion region is exposed to the surface, are far more sensitive to SRV, requiring substantially lower values of 10^3–10^4 cm/s to produce the same level of performance. For low values of the SRV (<100 cm/s), both axial and radial NWs can support V_{OC} values of >0.70 V if the bulk minority carrier lifetime is 1 µs or greater. Experimental measurements on NWs grown by a vapor–liquid–solid mechanism yield V_{OC} of 0.23 and 0.44 V for axial and radial NWs, respectively, and show that axial devices are limited by a SRV of ∼7 × 10^3 cm/s while radial devices are limited by a bulk lifetime of ∼3 ns. The simulations show that with further development the electrical characteristics of 200–300 nm Si NWs are sufficient to support power-conversion efficiencies of 15–25%. The analysis presented here can be generalized to other semiconductor homo- and heterojunctions, and we expect that insights from finite element modeling will serve as a powerful method to guide the design of advanced nanoscale structures.

- Trojan-Horse Nanotube On-Command Intracellular Drug Delivery
  Wu, C.-H.; Cao, C.; Kim, J. H.; Hsu, C.-H.; Wanebo, H. J.; Bowen, W. D.; Xu, J.; Marshall, J. *Nano Letters* **2012**, *12*, 5475-5480.
  Abstract:

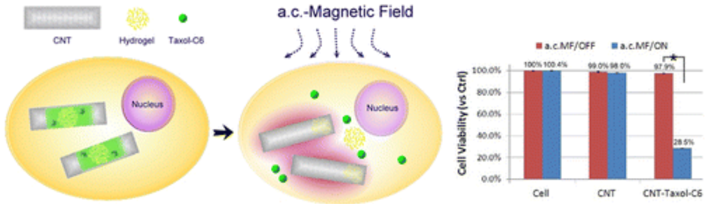

A major challenge to nanomaterial-based medicine is the ability to release drugs on-command. Here, we describe an innovative drug delivery system based on carbon nanotubes (CNTs), in which compounds can be released inside cells from within the nanotube “on-command” by inductive heating with an external alternating current or pulsed magnetic field. Without inductive heating the drug remains safely inside the CNTs, showing no toxicity in cell viability tests. Similar to the “Trojan-Horse” in function, we demonstrate the delivery of a combination of chemotherapeutic agents with low aqueous solubility, paclitaxel (Taxol), and C6-ceramide, to multidrug resistant pancreatic cancer cells. Nanotube encapsulation permitted the drugs to be used at a 100-fold lower concentration compared to exogenous treatment yet achieve a comparable ∼70% cancer kill rate.

- Degradable Thermoresponsive Polyesters by Atom Transfer Radical Polyaddition and Click Chemistry
  Zhang, L.-J.; Dong, B.-T.; Du, F.-S.; Li, Z.-C. *Macromolecules* **2012**, *45*, 8580–8587.
  Abstract:

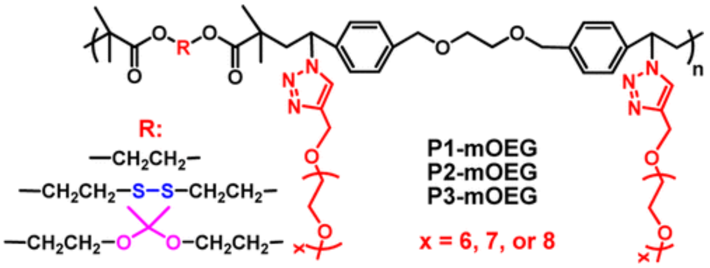

Three types of linear polyesters containing monodisperse methoxy oligo(ethylene glycol)s (mOEG, *x* = 6, 7, or 8) side chains (**P1-mOEG**, **P2-mOEG**, and **P3-mOEG**) have been synthesized by atom transfer radical polyaddition and click chemistry. Degradable disulfide and ketal groups were incorporated into the polymer backbone of **P2-mOEG** and **P3-mOEG** respectively. All of these three series of mOEG-grafted polyesters are water-soluble and display reversible thermoresponsive properties with tunable cloud point (CP). Aqueous solution properties and thermo-induced phase transitions were studied by ^{1}H NMR, turbidimetry, DLS, and fluorescence probe method. The results indicate that these polyesters mainly adopt single chain conformations in aqueous solution below CP. OEG length has a significant effect on the CP, the CP increases by ca. 10 °C when the repeating units of OEG side chains increase from 6 to 7, and by ca. 6 °C when they increase from 7 to 8. The main chain structures also affect the CP values, which decrease from **P1-mOEG** to **P3-mOEG** due to the increased hydrophobicity of the backbone. Degradation of the polymers was conducted under basic, reductive and mild acidic conditions, respectively. The degradation products also show thermoresponsive behaviors, but the CP values vary from the precursor polymers depending on the alteration of hydrophilic/hydrophobic balance and shielding effect of the OEG side chain.

- Donor–Acceptor Conjugated Polymers with Dithienocarbazoles as Donor Units: Effect of Structure on Semiconducting Properties
  Deng, Y.; Chen, Y.; Zhang, X.; Tian, H.; Bao, C.; Yan, D.; Geng, Y.; Wang, F. *Macromolecules* **2012**, *45*, 8621–8627.
  Abstract:

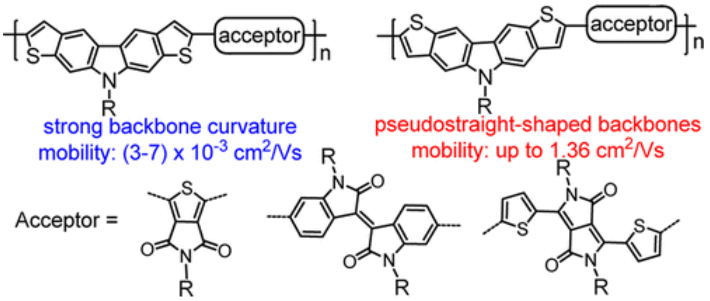

A series of donor–acceptor (D–A) conjugated polymers (CPs) comprising dithieno[2,3-*b*;7,6-*b*]carbazole (**C1**) or dithieno[3,2-*b*;6,7-*b*]carbazole (**C2**) as D unit and thienopyrroledione (**TPD**), isoindigo (**IID**), or diketopyrrolopyrrole (**DPP**) as A unit were synthesized, and their semiconducting properties were investigated with organic field-effect transistors (OFETs). Because of different bonding geometry of **C1** and **C2**, the CPs based on these isomeric D units have distinct backbone conformation. The CPs based on **C1** unit and all three A units show strong backbone curvature. In consequence, these polymers all formed amorphous films and exhibited low OFET mobility in the level of 10^{-3} cm^2/(V s). **P(TPD-C2)** and **P(DPP-C2)**, which comprise **C2** and **TPD** or **DPP**, both display pseudo-straight-shaped backbones and formed ordered films with the polymer backbones adopting edge-on orientation respective to the substrates. Accordingly, **P(TPD-C2)** and **P(DPP-C2)** exhibited the highest mobility of 0.31 and 1.36 $cm^2/(V\ s)$, respectively. However, **P(IID-C2)** could only form amorphous films probably owing to its highly stiff backbone, leading to a moderate OFET mobility (2.96×10^{-2} $cm^2/(V\ s)$). This implies that large fused aromatics are promising building blocks for high-mobility D–A CPs when polymer backbone conformation and rigidity are appropriately manipulated.

- Nanosized Optoelectronic Devices Based on Photoactivated Proteins
  Dimonte, A.; Frache, S.; Erokhin, V.; Piccinini, G.; Demarchi, D.; Milano, F.; De Micheli, G.; Carrara, S. *Biomacromolecules* **2012**, *13*, 3503–3509.
  Abstract:

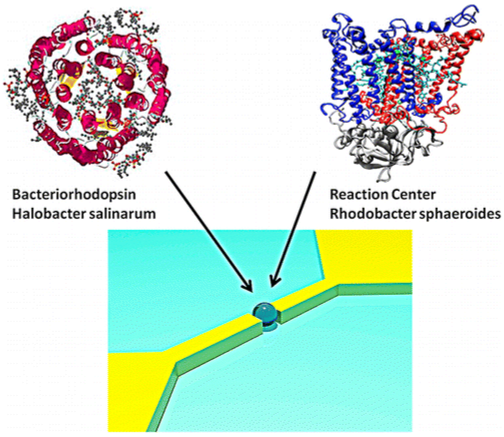

Molecular nanoelectronics is attracting much attention, because of the possibility to add functionalities to silicon-based electronics by means of intrinsically nanoscale biological or organic materials. The contact point between active molecules and electrodes must present, besides nanoscale size, a very low resistance. To realize Metal-Molecule-Metal junctions it is, thus, mandatory to be able to control the formation of useful nanometric contacts. The distance between the electrodes has to be of the same size of the molecule being put in between. Nanogaps technology is a perfect fit to fulfill this requirement. In this work, nanogaps between gold electrodes have been used to develop optoelectronic devices based on photoactive proteins. Reaction Centers (RC) and Bacteriorhodopsin (BR) have been inserted in nanogaps by drop casting. Electrical characterizations of the obtained structures were performed. It has been demonstrated that these nanodevices working principle is based on charge separation and photovoltage response. The former is induced by the application of a proper voltage on the RC, while the latter comes from the activation of BR by light of appropriate wavelengths.

- Double Smectic Self-Assembly in Block Copolypeptide Complexes
  Haataja, J. S.; Houbenov, N.; Iatrou, H.; Hadjichristidis, N.; Karatzas, A.; Faul, C. F. J.; Rannou, P.; Ikkala, O. *Biomacromolecules* **2012**, *13*, 3572–3580.
  Abstract:

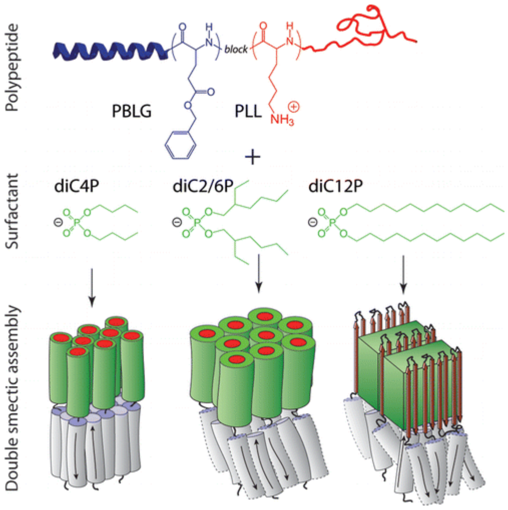

We show double smectic-like self-assemblies in the solid state involving alternating layers of different polypeptide α-helices. We employed rod–coil poly(γ-benzyl l-glutamate)-*block*-poly(l-lysine) (PBLG-*b*-PLL) as the polymeric scaffold, where the PLL amino residues were ionically complexed to di-*n*-butyl phosphate (diC4P), di(2-ethylhexyl) phosphate (diC2/6P), di(2-octyldodecyl) phosphate (diC8/12P), or di-*n*-dodecyl phosphate (diC12P), forming PBLG-*b*-PLL(diC4P), PBLG-*b*-PLL(diC2/6P), PBLG-*b*-PLL(diC8/12P), and PBLG-*b*-PLL(diC12P) complexes, respectively. The complexes contain PBLG α-helices of fixed diameter and PLL-surfactant complexes adopting either α-helices of tunable diameters or β-sheets. For PBLG-*b*-PLL(diC4P), that is, using a surfactant with short *n*-butyl tails, both blocks were α-helical, of roughly equal diameter and thus with minor packing frustrations, leading to alternating PBLG and PLL(diC4P) smectic layers of approximately perpendicular alignment of both types of α-helices. Surfactants with longer and branched alkyl tails lead to an increased diameter of the PLL-surfactant α-helices. Smectic alternating PBLG and PLL(diC2/6P) layers involve larger packing frustration, which leads to poor overall order and suggests an arrangement of tilted PBLG α-helices. In PBLG-*b*-PLL(diC8/12P), the PLL(diC8/12P) α-helices are even larger and the overall structure is poor. Using a surfactant with two linear *n*-dodecyl tails leads to well-ordered β-sheet domains of PLL(diC12P), consisting of alternating PLL and alkyl chain layers. This dominates the whole assembly, and at the block copolypeptide length scale, the PBLG α-helices do not show internal order and have poor organization. Packing frustration becomes an important aspect to design block copolypeptide assemblies, even if frustration could be relieved by conformational imperfections. The results suggest pathways to control hierarchical liquid-crystalline assemblies by competing interactions and by controlling molecular packing frustrations.

- Advances in self-healing optical materials
  Amendola, V.; Meneghetti, M. *J. Mater. Chem.* **2012**, *22*, 24501–24508.
  Abstract:

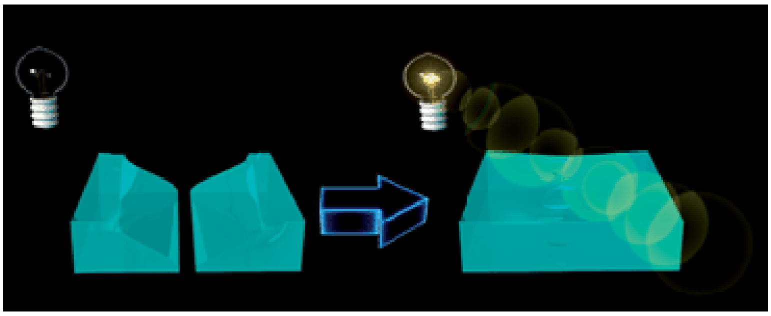

In recent years, new approaches for the self-repair of optical materials have been proposed, in particular for transparent coatings and systems for solar energy conversion. Moreover, light has been exploited for remotely triggering self-healing in optically responsive materials. This ambitious goal required state of the art knowledge in different disciplines and fine engineering of materials architecture. Here we highlight the recent advances in the field and provide some possible directions for the near future.

- Synthesis of a New Ladder-Type Benzodi(cyclopentadithiophene) Arene with Forced Planarization Leading to an Enhanced Efficiency of Organic Photovoltaics
  Chen, Y.-L.; Chang, C.-Y.; Cheng, Y.-J.; Hsu, C.-S *Chem. Mater.* **2012**, *24*, 3964–3971.
  Abstract:

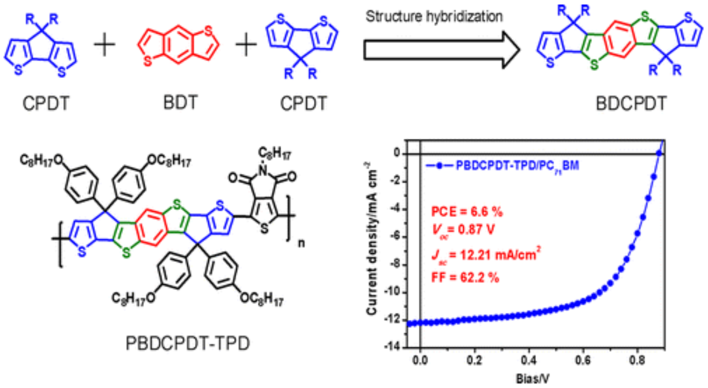

We have developed a new heptacyclic benzodi(cyclopentadithiophene) (**BDCPDT**) unit, where 3,7-positions of the central benzo[1,2-*b*:4,5-*b*′]dithiophenes (**BDT**) subunit are covalently rigidified with 3-positons of the two external thiophenes by two carbon bridges, forming two external **CPDT** rings that share two thiophene rings with the central **BDT** core. The distannyl-**BDCPDT** building block was copolymerized with 1,3-dibromo-thieno[3,4-*c*]pyrrole-4,6-dione (**TPD**) by Stille polymerization to afford a new alternating donor–acceptor copolymer **PBDCPDT-TPD**. The implementation of forced planarization greatly suppresses the interannular twisting to extend the effective conjugated length and preserve the interactions between the donor and acceptor segments. The device using the **PBDCPDT-TPD**/PC$_{71}$BM (1:3 in wt%) blend processed with dimethyl sulfoxide as an additive delivered a marked PCE of 6.6% which represents a significant enhancement compared to the device using the corresponding nonfused polymer analogue with a PCE of 0.2%.

- Orthogonal supramolecular interaction motifs for functional monolayer architectures
  Yilmaz, M. D.; Huskens, J. *Soft Matter* **2012**, *8*, 11768-11780.
  Abstract:

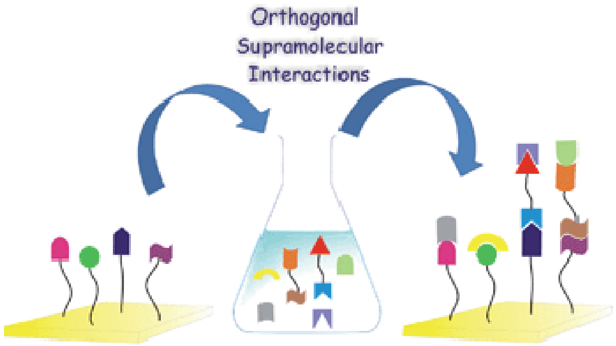

Organization of molecules on surfaces is of utmost importance for the construction of functional materials. Non-covalent, weak and reversible supramolecular interactions provide this organization with high specificity and selectivity. The integration of different supramolecular systems is essential for the assembly of complex and functional architectures on surfaces. Self-assembly, in particular orthogonal self-assembly, is the main route to achieve these integrated architectures. This review article gives an overview of the recent developments of orthogonal supramolecular interactions on surfaces. The first part deals with the use of noncovalent interactions, including hydrogen bonding, metal coordination, electrostatics and host–guest interactions, to modify surfaces. The second part describes the combination of different orthogonal supramolecular interaction motifs for the generation of hybrid assemblies and materials.

- Interface cross-linked polymeric micelles with mixed coronal chains prepared by RAFT polymerization at the interface
  Jin, J.; Zhang, M.; Xiong, Q.; Sun, P.; Zhao, H. *Soft Matter* **2012**, *8*, 11809-11816.
  Abstract:

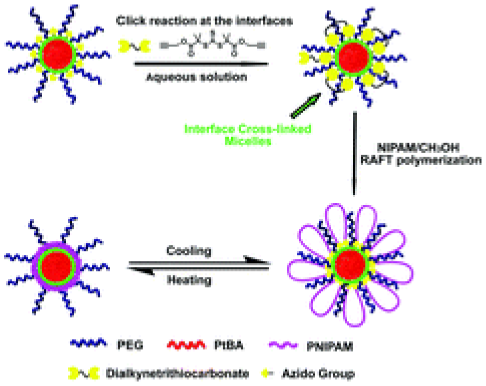

Poly(ethylene glycol-*block*-2-hydroxyethyl methacrylate-*block*-*tert*-butyl acrylate) (PEG-*b*-PHEMA-*b*-P*t*BA) triblock copolymer was synthesized by the sequential atom transfer radical polymerization (ATRP) of HEMA and *t*BA using an ATRP initiator terminated PEG (PEG-Br) as the macroinitiator. Azide groups were introduced to the short mid-blocks by reactions of the triblock copolymer with 2-bromoisobutyryl bromide and sodium azide. In aqueous solution, the triblock copolymer self-assembled into micelles with azide groups at the interfaces. Reactive polymeric micelles with reversible addition–fragmentation chain transfer agents (RAFT CTAs) at the interfaces were prepared by a click cross-linking reaction between dialkynetrithiocarbonate and the azide groups. FT-IR, ^{1}H NMR, dynamic light scattering (DLS) and transmission electron microscopy (TEM) were used to characterize the interface cross-linked (ICL) micelles and the grafting of the RAFT CTAs to the interfaces. Polymeric micelles with PEG–poly(*N*-isopropylacrylamide) (PNIPAM) mixed coronal chains were prepared by the *in situ* RAFT polymerization of NIPAM at the interfaces. The TEM results demonstrate that the mixed coronal chains have nano-sized phase separation on the surfaces of the micelles. The use of the polymeric micelles as particulate emulsifiers was also investigated in this research. These ICL micelles with mixed coronal chains produce relatively fine 1-undecanol-in-water (o/w) emulsions compared to emulsions stabilized by the PEG homopolymer under the same conditions.

- Magnetic Nanoparticles: Design and Characterization, Toxicity and Biocompatibility, Pharmaceutical and Biomedical Applications
  Reddy, L. H.; Arias, J. L.; Nicolas, J.; Couvreur, P. *Chem. Rev.* **2012***, 112*, 5818-5878.

Abstract:

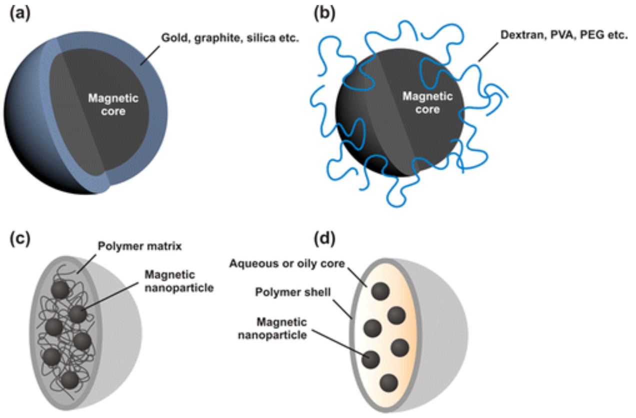

This review will comprehensively describe the synthesis of MNPs, their physicochemical characterization, and their biopharmaceutical performances, including pharmacokinetics, biodistribution, and toxicity. A particular emphasis will be given to their applications in therapy, diagnosis, tissue engineering, and other biomedical applications such as sensing and separation of cells, bacteria and viruses, and analysis of biochemicals and heavy metals.

- The Conundrum of pH in Water Nanodroplets: Sensing pH in Reverse Micelle Water Pools
  Crans, D. C.; Levinge, N. E. *Acc. Chem. Res.* **2012**, *45*, 1637-1645**.**
  Abstract:

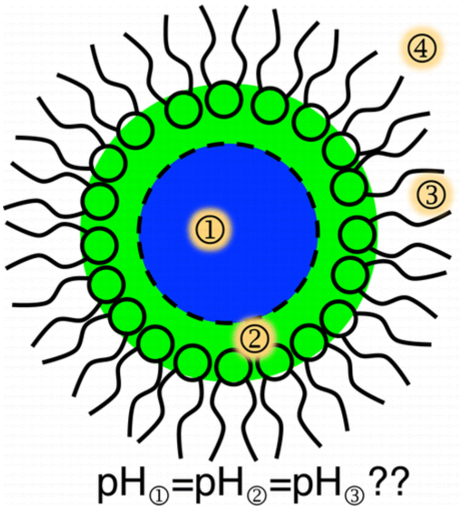

In aqueous environments, acidity is arguably the most important property dictating details of chemistry that can occur. As the size of systems decreases, the number of water molecules becomes limited to a very small proportion and the conventional macroscopic description no longer applies. Various experimental approaches have characterized nanoscale water using probes with spectroscopic signatures observable by UV–vis spectroscopy, fluorescence spectroscopy, and NMR spectroscopy. Here we describe issues surrounding the concept of acidity and pH in the water pools of reverse micelles with fewer than 10^7 water molecules. We also summarize our studies probing pH and its effects on these systems and reactions in confined spaces.

- Controllable Self-Assembly of Di(p-methoxylphenyl)Dibenzofulvene into Three Different Emission Forms
  Gu, X.; Yao, J.; Zhang, G.; Zhang, D. *Small* **2012**, *8*, 3406–3411.

<u>Abstract:</u>

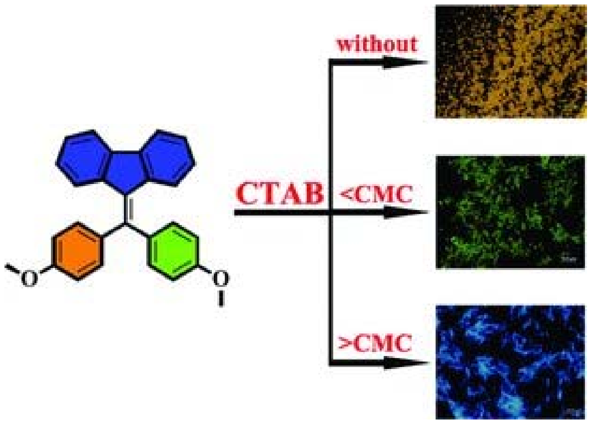

Self-assembly of di(p-methoxylphenyl)dibenzofulvene in the absence and presence of CTAB (cetyl trimethylammonium bromide) leads to three emission forms: strongly yellow-green- and blue-emissive crystalline forms (as microrods), and weakly orange-emissive amorphous form. Each of these three emission forms can be prepared by adjusting the concentration of CTAB.

- Self-Assembled Block Copolymer–Nanoparticle Hybrids: Interplay between Enthalpy and Entropy
  Sarkar, B.; Alexandridis, P. *Langmuir* **2012**, *28*, 15975–15986.
  <u>Abstract:</u>

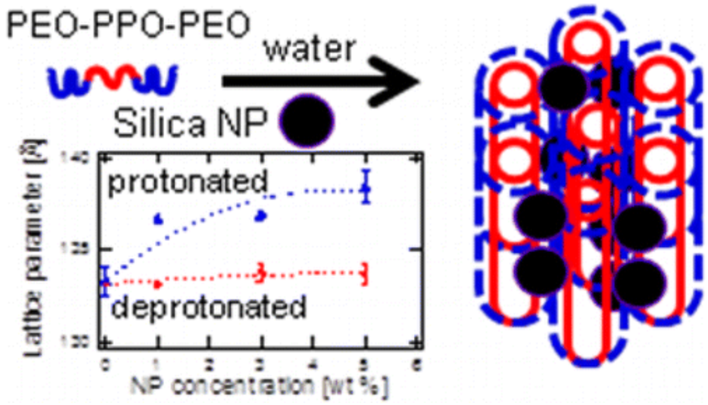

The dispersion of nanoparticles in ordered block copolymer nanostructures can provide control over particle location and orientation, and pave the way for engineered nanomaterials that have enhanced mechanical, electrical, or optical properties. Fundamental questions pertaining to the role of enthalpic and entropic particle–polymer interactions remain open and motivate the present work. We consider here a system of 10.6 nm silica nanoparticles (NPs) dispersed in ordered cylinders formed by hydrated poly(ethylene oxide)–poly(propylene oxide) block copolymers (Pluronic P105: EO37PO56EO37). Protonation of silica was used to vary the NP–polymer enthalpic interactions, while polar organic solvents (glycerol, DMSO, ethanol, and DMF) were used to modulate the NP–polymer entropic interactions. The introduction of deprotonated NPs in the place of an equal mass of water did not affect the lattice parameter of the PEO-PPO-PEO block copolymer hexagonal lyotropic liquid crystalline structures. However, the dispersion of protonated NPs led to an increase in the lattice parameter, which was attributed to stronger NP–polymer hydrogen bonding (enthalpic) interactions. Dispersion of protonated NPs into cylindrical structures formed by Pluronic P105 in 80/20 water/organic solvents does not influence the lattice parameter, different from the case of protonated NP in plain water. Organic solvents appear to screen the NP–polymer hydrogen bonding interactions.

- Hierarchically Structured Porous Materials for Energy Conversion and Storage
  Li, Y.; Fu, Z.-Y.; Su, B.-L. *Adv. Funct. Mater.* **2012**, *22*, 4634–4667.
  Abstract:

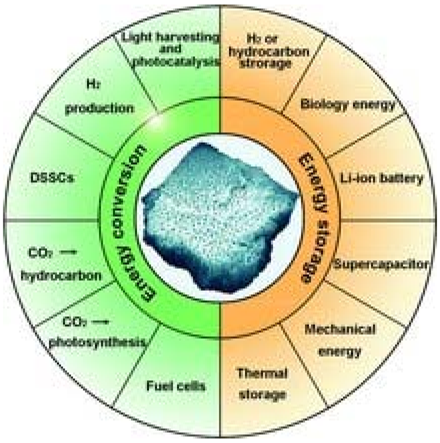

Materials with hierarchical porosity and structures have been heavily involved in newly developed energy storage and conversion systems. Because of meticulous design and ingenious hierarchical structuration of porosities through the mimicking of natural systems, hierarchically structured porous materials can provide large surface areas for reaction, interfacial transport, or dispersion of active sites at different length scales of pores and shorten diffusion paths or reduce diffusion effect. By the incorporation of macroporosity in materials, light harvesting can be enhanced, showing the importance of macrochannels in light related systems such as photocatalysis and photovoltaics. A state-of-the-art review of the applications of hierarchically structured porous materials in energy conversion and storage is presented. Their involvement in energy conversion such as in photosynthesis, photocatalytic H_2 production, photocatalysis, or in dye sensitized solar cells (DSSCs) and fuel cells (FCs) is discussed. Energy storage technologies such as Li-ions batteries, supercapacitors, hydrogen storage, and solar thermal storage developed based on hierarchically porous materials are then discussed. The links between the hierarchically porous structures and their performances in energy conversion and storage presented can promote the design of the novel structures with advanced properties.

- Hierarchically Structured Superoleophobic Surfaces with Ultralow Contact Angle Hysteresis
  Kota, A. K.; Li, Y.; Mabry, J. M.; Tuteja, A. *Adv. Mater.* **2012**, *24*, 5838–5843.
  Abstract:

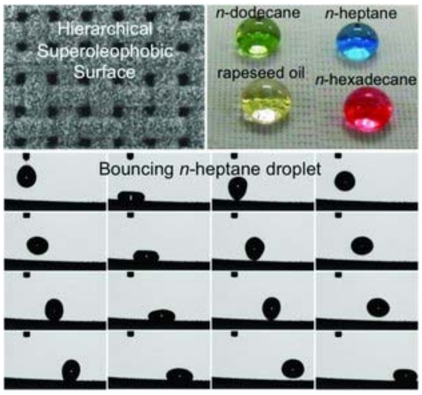

Hierarchically structured, superoleophobic surfaces are demonstrated that display one of the lowest contact angle hysteresis values ever reported – even with extremely low-surface-tension liquids such as *n*-heptane. Consequently, these surfaces allow, for the first time, even ≈2 μL *n*-heptane droplets to bounce and roll-off at tilt angles. ≤ 2°.

- From metamaterials to metadevices
  Zheludev, N. I.; Kivshar, Y. S. *Nature Materials* **2012**, *11*, 917–924.
  Abstract:

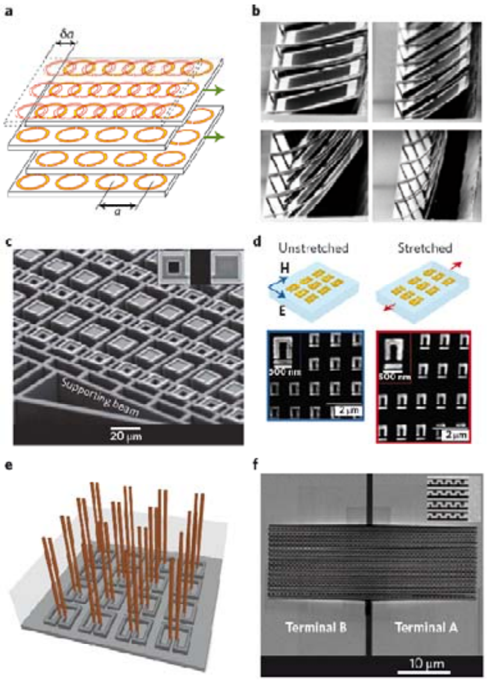

Metamaterials, artificial electromagnetic media that are structured on the subwavelength scale, were initially suggested for the negative-index 'superlens'. Later metamaterials became a paradigm for engineering electromagnetic space and controlling propagation of waves: the field of transformation optics was born. The research agenda is now shifting towards achieving tunable, switchable, nonlinear and sensing functionalities. It is therefore timely to discuss the emerging field of metadevices where we define the devices as having unique and useful functionalities that are realized by structuring of functional matter on the subwavelength scale. In this Review we summarize research on photonic, terahertz and microwave electromagnetic metamaterials and metadevices with functionalities attained through the exploitation of phase-change media, semiconductors, graphene, carbon nanotubes and liquid crystals. The Review also encompasses microelectromechanical metadevices, metadevices engaging the nonlinear and quantum response of superconductors, electrostatic and optomechanical forces and nonlinear metadevices incorporating lumped nonlinear components.

- Nanostructured high-energy cathode materials for advanced lithium batteries
  Sun, Y-K.; Chen, Z.; Noh, H-J.; Lee, D-J.; Jung, H-G.; Ren, Y.; Wang, S.; Yoon, C. S.; Myung, S-T.; Amine, K. *Nature Materials* **2012**, *11*, 942–947.
  Abstract:

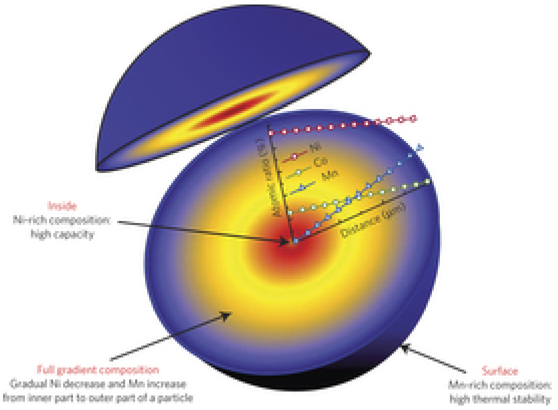

Nickel-rich layered lithium transition-metal oxides, LiNi1−xMxO2 (M = transition metal), have been under intense investigation as high-energy cathode materials for rechargeable lithium batteries because of their high specific capacity and relatively low cost1, 2, 3. However, the commercial deployment of nickel-rich oxides has been severely hindered by their intrinsic poor thermal stability at the fully charged state and insufficient cycle life, especially at elevated temperatures. Here, we report a nickel-rich lithium transition-metal oxide with a very high capacity (215 mA h g−1), where the nickel concentration decreases linearly whereas the manganese concentration increases linearly from the centre to the outer layer of each particle. Using this nano-functional full-gradient approach, we are able to harness the high energy density of the nickel-rich core and the high thermal stability and long life of the manganese-rich outer layers. Moreover, the micrometre-size secondary particles of this cathode material are composed of aligned needle-like nanosize primary particles, resulting in a high rate capability. The experimental results suggest that this nano-functional full-gradient cathode material is promising for applications that require high energy, long calendar life and excellent abuse tolerance such as electric vehicles.